

# Insights into proton translocation in cbb3 oxidase from MD simulations

Carvalheda , Catarina A.; Pisliakov, Andrei V.

*Published in:*
Biochimica et Biophysica Acta (BBA) - Bioenergetics

*DOI:*
10.1016/j.bbabio.2017.02.013

*Publication date:*
2017

*Document Version*
Peer reviewed version


# Insights into proton translocation in *cbb*$_3$ oxidase from MD simulations

Catarina A. Carvalheda, Andrei V. Pisliakov

PII: S0005-2728(17)30041-5
DOI: doi:10.1016/j.bbabio.2017.02.013
Reference: BBABIO 47791

To appear in: *BBA - Bioenergetics*

Received date: 5 October 2016
Revised date: 3 February 2017
Accepted date: 27 February 2017

Please cite this article as: Catarina A. Carvalheda, Andrei V. Pisliakov, Insights into proton translocation in *cbb*$_3$ oxidase from MD simulations, *BBA - Bioenergetics* (2017), doi:10.1016/j.bbabio.2017.02.013

# Insights into proton translocation in *cbb*$_3$ oxidase from MD simulations

Catarina A. Carvalheda[ab*], Andrei V. Pisliakov[ab*]

[a]Computational Biology, School of Life Sciences, University of Dundee, Dow Street, Dundee, DD1 5EH, United Kingdom

[b]Physics, School of Sciences and Engineering, University of Dundee, Nethergate, Dundee, DD1 4HN, United Kingdom

## Abstract

Heme-copper oxidases are membrane protein complexes that catalyse the final step of the aerobic respiration, namely the reduction of oxygen to water. The energy released during catalysis is coupled to the active translocation of protons across the membrane, which contributes to the establishment of an electrochemical gradient that is used for ATP synthesis. The distinctive C-type (or $cbb_3$) cytochrome *c* oxidases, which are mostly present in proteobacteria, exhibit a number of unique structural and functional features, including high catalytic activity at low oxygen concentrations. At the moment, the functioning mechanism of C-type oxidases, in particular the proton transfer/pumping mechanism presumably via a single proton channel, is still poorly understood. In this work we used all-atom molecular dynamics simulations and continuum electrostatics calculations to obtain atomic-level insights into the hydration and dynamics of a $cbb_3$ oxidase. We provide the details of the water dynamics and proton transfer pathways for both the "chemical" and "pumped" protons, and show that formation of protonic connections is strongly affected by the protonation state of key residues, namely H243, E323 and H337.



Keywords: molecular dynamics simulations, p$K_a$ calculations, proton transfer, water dynamics, cytochrome *c* oxidase, proton pump, membrane protein



## *Corresponding author:

Email addresses: c.a.c.dossantos@dundee.ac.uk, a.pisliakov@dundee.ac.uk

# 1. Introduction

Heme-copper oxidases (HCOs) terminate the respiratory chain of most aerobic organisms. In a stepwise manner, HCOs catalyse the reduction of oxygen to water and use the redox energy generated during catalysis to actively pump protons from the negative to the positive side of the membrane, thereby contributing to the formation of an electrochemical gradient used for ATP synthesis [1–4]. According to their structural and functional features oxidases can be divided into three families: type A ($aa_3$, mitochondrial-like), type B ($ba_3$) and type C ($cbb_3$) oxidases [5–7]. All HCOs share the same architecture for the central subunit (subunit I or CcoN in C-type), containing 12 membrane-spanning helices and an active centre composed of a low-spin heme and a high-spin heme – copper binuclear centre (BNC) coordinated by conserved histidine residues. The canonical A-type are the most studied oxidases. These are present in all the three domains of life, while the B-type are mostly found in archea and C-type predominantly in bacteria. Notably, the A-type oxidases have two proton pathways (so-called D- and K-channel), which are used for chemical and pumped protons, while B- and C-type have a single proton pathway located in the same region as the K-channel of A-type oxidases (see details below) [3].

C-type cytochrome *c* oxidases are a highly divergent group and the least studied members of the HCO superfamily. They exhibit a number of unique features, such as high affinity for $O_2$, and thus high catalytic activity at low oxygen concentrations, and ability to reduce nitric oxide under anaerobic conditions, along with some structural resemblance to the *bona fide* nitric oxide reductases (NORs) [8,9]. The prototype of the C-family is a cytochrome $cbb_3$ oxidase. Importantly, it is the only terminal oxidase expressed in some clinically relevant human pathogens (e.g. *Campylobacter jejuni* and *Helicobacter pylori*), and thus it is required for microaerobic respiration and colonisation of anoxic tissues. This makes $cbb_3$ a potential target for therapeutic purposes.

The first $cbb_3$ structure containing all core subunits ($cbb_3$ from *Pseudomonas stutzeri*) was solved by Buschmann *et al.* at a 3.4 Å resolution [10]. Four chains were resolved in that structure: three core subunits – subunits N (CcoN or I), O (CcoO or II) and P (CcoP or III) – which are essential for the enzymatic activity (Figure 1A), and subunit M (CcoM) that was recently shown to have a putative role in the $cbb_3$ complex assembly and stability [11]. The central subunit CcoN, was shown to have the same overall architecture as in A- and B-type oxidases, with an active site composed of a heme $b_3$ – $Cu_B$ binuclear centre (Figure 1D). The

highly conserved tyrosine, which is crosslinked to one of histidine ligands of $Cu_B$ (H207 in *P. stutzeri*), is also present in this structure, though it is located in a different helix as was predicted previously [12]. Unlike most A- and B-type oxidases, which contain an additional copper centre, $Cu_A$, located in the hydrophilic part of subunit II, $cbb_3$ contains three extra hemes (all type *c*) embedded in the hydrophilic domain of subunits CcoO and CcoP. This results in a distinctly different electron transfer (ET) mechanism that includes: outer and inner heme *c* in subunit CcoP, heme *c* in subunit CcoO, and heme *b* and the BNC in subunit CcoN, as shown schematically in Figure 1B [10]. In resemblance to the known NORs [13,14], the heme *b* and heme $b_3$ groups are bridged by a calcium ion, instead of two arginine residues that are conserved in all A- and B-type oxidases. Furthermore, the proximal ligand of heme $b_3$, H345, is H-bonded to E323, which is another structural feature of $cbb_3$ oxidases. Two internal cavities were identified in $cbb_3$ (Figure 1C): i) a (hydrophilic) periplasmic cavity extending more than 15 Å from the BNC to the postulated exit to the periplasm, which is absent in other structurally known oxidases and was suggested be part of the proton exit pathway, and ii) a (hydrophobic) membrane cavity that likely serves for oxygen to the active site, and is similar to the one found in B-family, and is located in a position equivalent to the end of the D-channel in A-type oxidases. The unique structural and functional features of $cbb_3$ oxidases described above suggest that there could be significant differences in the way they carry out their function, i.e. oxygen reduction and proton pumping.

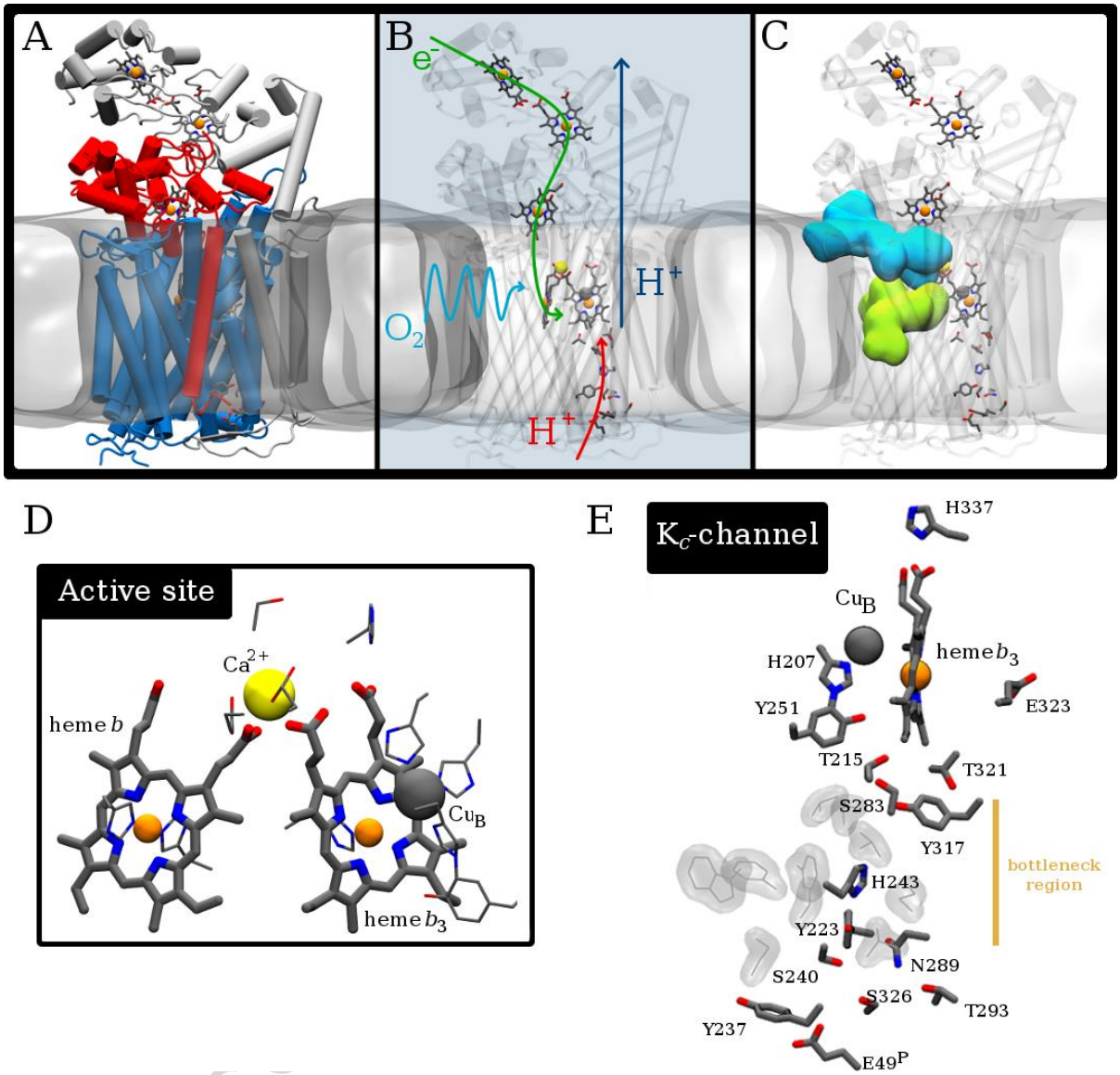


Figure 1. Overall architecture and main functional elements of *cbb*$_3$ oxidase. **(A)** *cbb*$_3$ oxidase embedded in membrane. Subunits CcoN (blue), CcoO (red) and CcoP (grey) comprise the protein complex. **(B)** Schematic illustration of the electron, oxygen and proton pathways. **(C)** Hydrophilic (cyan) and hydrophobic (green) internal cavities. **(D)** Organisation of the active site. **(E)** A proton pathway ($K_c$-channel) connects the cytoplasmic side of the membrane with the active site. The residues E323 and H337 are proposed to be part of the proton loading site and/or exit pathway. The relevant residues and cofactors are shown as sticks, while the copper centre ($Cu_B$), iron ions of hemes and calcium ion bridging hemes *b* and $b_3$ are represented as spheres. The single-letter amino acid abbreviations are used. The lipid bilayer membrane is represented as a transparent grey surface in panels A to C. The protein structure is shown as a transparent grey cartoon in panels B and C. The bulk water is represented as a transparent blue surface in panel B. The hydrophobic ring around H243 is represented as a grey transparent surface and lines in panel E.

Long-range proton transfer in proteins is usually described by a Grotthuss-like mechanism, according to which protons are translocated in a stepwise manner along well specified pathways that are stabilized by polar groups [1,15,16]. In *cbb*$_3$ a single proton channel from the cytoplasmic side transports both chemical and pumped protons [10,12,17–21]. This is referred to as $K_c$-channel, as it is positioned equivalently to the K-channel in A-type. The highly conserved residue E49 in subunit CcoP ($E25^P$ in *Rhodobacter sphaeroides*) was shown

to be an entry point to this channel [17,22]. The further $K_c$ pathway towards the BNC is lined by the residues Y237, S236, T293, S240, N289, Y223, H243, Y317, S283, T215, Y251 (*P. stutzeri* numbering; residues of the main subunit, CcoN, are listed without superscript) [10,12,17–21], with a bottleneck region centred on H243, which sits in the narrowest part of the channel surrounded by a ring of hydrophobic residues (Figure 1E). No D-channel analogue was identified in $cbb_3$ [10,18].

For efficient proton pumping, a gating mechanism should be in place to prevent proton leaking [2–4,23]. The models of proton pumping by oxidases usually include a redox-controlled "proton loading site" (PLS), which can accept and store protons during some steps of the catalytic cycle, before releasing them to the positive side of the membrane. Different candidates, all located close to the BNC towards the positive side of the membrane, where considered for this role, namely D- and A-propionate of heme $a_3$, water molecule, or the water cluster – in A-type [23–32] and A propionate and nearby residues – in B-type [33–40] oxidases. Two possible proton exit pathways were previously suggested for $cbb_3$ [10,41]. The first involves E125 (which coordinates the calcium ion that clamps heme *b* and heme $b_3$ together) and E122 (which sits in the periplasmic cavity) [10], which are highly conserved in both $cbb_3$ oxidases and NORs [42]. The second involves a unique route "behind" the active site heme along the residues Y317, T321, S320, E323 and reaches the A-propionate of heme $b_3$ [41]. The latter proposal also suggests Y317 as the branching point from where the chemical and pumped protons split and are either delivered to the active site for oxygen reduction or to the proximal side of heme $b_3$ and (unknown) PLS for pumping, which is in agreement with experimental observations [21]. Such exit pathway could possibly involve redox-induced $pK_a$ shifts in E323 (H-bonded to the proximal ligand of heme $b_3$) and/or H337 (interacting with A-propionate of heme $b_3$ and highly conserved in C-type oxidases) [41].

Atomic insights into the mechanism of proton translocation in proteins can be obtained by computational methods, as e.g. was extensively shown in studies of cytochrome *c* oxidases [1,28,43–48]. These studies predominantly focused on A-type oxidases. Only two previous computational works reported the analysis of water dynamics in $cbb_3$ [17,41], which greatly contributed to the present understanding of the proton pathways in the enzyme. Sharma *et al.* [41] studied the dynamics of internal water networks in the $K_c$-channel and in a plausible proton exit pathway via E323 (described above). However, the simulation system in that study comprised only two subunits, CcoN and CcoO, thus excluding subunit CcoP and the critical $E49^P$ residue, and did not include explicit membrane or solvent. Furthermore, the

reported timescale was very short (about 5 ns). Therefore it is not clear whether or not the observed water networks were a result of the insertion of internal water molecules during the system setup. The computational part of the study by Ahn *et al.* [17] focused only on the entrance region of the $K_c$-channel. The authors highlighted the role of $E49^P$ in the proton uptake to the channel and proposed a channel opening-closing mechanism governed by sidechain conformational changes of $E49^P$ and Y237.

In this work we perform large-scale all-atom molecular dynamics (MD) simulations of $cbb_3$ oxidase containing three core subunits within an explicit lipid bilayer membrane and solvent. MD simulations are complemented by continuum electrostatics p$K_a$ calculations. We focus on the details of the proton translocation pathways, the $K_c$-channel and plausible pumping pathway, and explore the effect of the protonation state of the key residues and mechanistic details of the channel formation. We identify the likely candidate for the proton loading site and propose a model of the proton pumping/gating mechanism. We also model the effect of four previously reported mutations, which reduce the activity or decouple the proton pumping.

# 2. Materials and Methods

## 2.1. System setup and MD settings

The initial protein coordinates were obtained from the crystal structure of $cbb_3$ oxidase from *Pseudomonas stutzeri* (PDB ID code: 3MK7) [10]. Subunits CcoN, CcoO and CcoP (corresponding to chains A, B and C in the PDB file), were used in the current work. The partial charges for the redox centres (hemes *c*, heme *b*, heme $b_3$ and $Cu_B$) were obtained using Gaussian03 [49] and Ambertools14 [50], as described in the Supplementary Material. The calculated charges were used in MD simulations and continuum electrostatics calculations (see below). Internal waters in the initial structure were modelled with DOWSER [51] using a binding free energy threshold of -10 kcal/mol, which resulted in the insertion of 166 internal water molecules, most of them in the hydrophilic cavity "above" the active site (shown in Figure 1C). In agreement with previous studies [10,17], only four DOWSER waters were predicted in the $K_c$-channel: three in the top region and one at the entrance (between $E49^P$ and S240). The protein was then inserted in an equilibrated POPE lipid bilayer using LAMBADA and InflateGRO2 [52], resulting in a membrane-protein system

containing 413 lipid molecules. The system was solvated using the TIP3P water molecules [53], and neutralized with $Na^+$ ions. The total system size was ~200 K atoms. No ionic concentration was used. Both calcium ions seen in the crystal structure were kept; their positions and coordination remained very stable throughout our simulations. The only exception was S102 which coordinates the calcium ion between two hemes in the crystal structure but moves away and is replaced by a water molecule in MD simulations (data not shown). The protonation state of ionisable residues was assigned according to continuum electrostatics calculations by a Poisson-Boltzmann/Monte Carlo approach, using MEAD (version 2.2.9) [54] and MCRP [55] as described in detail in the Supplementary Material. Based on predictions from continuum electrostatics calculations, all ionisable residues were modelled in their default protonation states (i.e. -1 for Asp and Glu, and +1 for Arg and Lys), except for E323, which was simulated in both charged and neutral states. All histidine residues were taken neutral, except for H124 in subunit CcoO, which was predicted protonated, and H243 and H377, which were simulated in both charged and neutral states. The heme centres were modelled in the reduced state and the copper centre was modelled with a hydroxyl as a fourth ligand. All MD simulations were performed with GROMACS version 5.0.2 [56,57], using the CHARMM36 force field [58–60] and in-house parameterization for the redox sites. The solvated protein-membrane systems were energy minimized, equilibrated and simulated according to the protocol described in the Supplementary Material. To ensure proper statistics, we performed three runs for each simulation system. In simulation systems A and B, replicas were generated using different initial velocities. In simulations C, D and E, the final configurations of simulations B1-3 were taken as the initial coordinates for the extended simulations, and the alterations – change of protonation state of H243, H337 and E323, respectively – were introduced as described in Table 1. For example, simulation C1* represents an extension of simulation B1 with the charge of H243 changed to 0. After changing the protonation state, a short (0.1 ps) equilibration was performed, during which the protein and membrane were kept rigid, allowing solvent molecules to adapt to the new charge configuration, similar to the constant-pH MD method [61]. In simulations C1*-3*, H243 was changed from the charged form (HSP in CHARMM) to the neutral form in which the imidazole nitrogen $N^{\varepsilon}$ is deprotonated (HSD). In simulations D1*-3*, H337 was converted to the neutral form in which the imidazole nitrogen $N^{\delta}$ is deprotonated (HSE). A summary of the simulations performed in this work is presented in Table 1, including simulations performed for the mutant variants H243G,

E49$^{P}$A, T215A and Y317F. Mutants were created using PyMOL [62] and two replicas were run for each variant.

**Table 1.** Summary of MD simulations performed in this work. The protonation state of the key residues H243, E323, and H337 is specified (His: "0" – neutral, deprotonated, "+" – positively charged, protonated; Glu: "-" – negatively charged, deprotonated, "0" – neutral, protonated). Asterisk (*) denotes the calculations that have been extended from the final snapshot of the previous simulation (B1-3) after changing the protonation state of a key residue.

| Simulation | | H243 | E323 | H337 | Length (ns) |
|---|---|---|---|---|---|
| A | 1 | 0 | – | + | 356 |
| | 2 | | | | 340 |
| | 3 | | | | 300 |
| B | 1 | + | – | + | 300 |
| | 2 | | | | 300 |
| | 3 | | | | 300 |
| C | 1* | 0 | – | + | 50 |
| | 2* | | | | 50 |
| | 3* | | | | 50 |
| D | 1* | + | – | 0 | 150 |
| | 2* | | | | 250 |
| | 3* | | | | 250 |
| E | 1* | + | 0 | + | 100 |
| | 2* | | | | 100 |
| | 3* | | | | 100 |
| H243G | R1 | + | – | + | 200 |
| | R2 | | | | 200 |
| E49$^{P}$A | R1 | + | – | + | 200 |
| | R2 | | | | 200 |
| T215A | R1 | + | – | + | 200 |
| | R2* | | | | 200 |
| Y317F | R1 | + | – | + | 200 |
| | R2 | | | | 200 |
| | | | Total simulation time: | | **4,596 ns** |

## 2.2. Analysis

All the analyses were performed using GROMACS tools and VMD [63]. The root-mean square deviation (rmsd) and root-mean-square fluctuation (rmsf) were calculated after least-squares fit of the $C_\alpha$ atoms of the transmembrane region to the reference structure (initial configuration at t = 0 ns). For the rmsf and water occupancy maps only the equilibrated part of the trajectories was taken into account: >25 ns for simulations A, B and mutants, and >5 ns for simulations C, D and E. The water occupancy maps were calculated using the Volmap

tool in VMD with a 0.5 Å resolution grid for water molecules within 4 Å of selected residues. The resulting volumetric maps are shown as an isosurface (mesh representation) with an isovalue of 0.15 (i.e. representing the regions with a water occupancy ≥15 %) in all cases. In some analyses the $K_c$-channel was sub-divided into three regions, which are referred to as top, bottom and bottleneck. The top part includes the residues H207, T215, Y251, S283, Y317, S320, T321, H345, the bottom – Y223, S236, Y237, S240, H243, N289, T293, and the bottleneck – Y223, H243, N289, Y317. An additional selection, called the bifurcation region, includes the residues S320, T321 and H345.

# 3. Results and Discussion

## 3.1. $K_c$-channel hydration and protonation state of H243

As mentioned in the Introduction, $K_c$-channel is the only proton uptake pathway identified in $cbb_3$ oxidases [10,12,17–21]. It provides a connection between the cytoplasm and the active site. The channel is formed by a number a polar residues and has a bottleneck region around H243, which is surrounded by a ring of nonpolar residues (Figure 1E). Based on our p$K_a$ calculations (data not shown) H243 is always predicted to be neutral, exhibiting significant negative p$K_a$ shifts from its model value. However, given that H243 sits in the narrowest part of the channel and is the only ionisable residue in the region, its direct involvement in the proton translocation is very likely. Therefore, we performed simulations for both neutral ("0", deprotonated) and charged ("+", protonated) forms of H243 – simulations A and B, respectively (Table 1). In the simulations A1-3 (with H243 neutral) we observed a discontinuous water chain in the $K_c$-channel, with a wide gap around H243 and Y233 (Figure 2A and S2A). In contrast, in the simulations B1-3 (with H243 positively charged) we consistently observed a continuous and stable water chain connecting the cytoplasmic side of the membrane to the active site (Figure 2B and S2B). We further analysed the hydration of different parts of the $K_c$-channel and found that the main difference between the simulations A and B comes from the bottom and bottleneck regions of the $K_c$-channel. The effect of the H243 charge is clear when comparing the number of waters in these two regions (Figure 2C and D). Although an initial influx of water molecules is observed in both cases, only when H243 is charged the waters populate the bottleneck region (on average ~7 waters when H243 is charged vs only ~2 waters when H243 is neutral) and form a connection to the top part of the channel (Figure 2). The water dynamics in the top part is less sensitive to the charge of

H243. It should be noted that only four waters were initially placed by DOWSER in the $K_c$-channel (see section 2.1). In simulations A1-3 only the waters placed in the top part remained in the channel, while in simulations B1-3 extra waters arrived from the cytoplasmic side of the membrane.

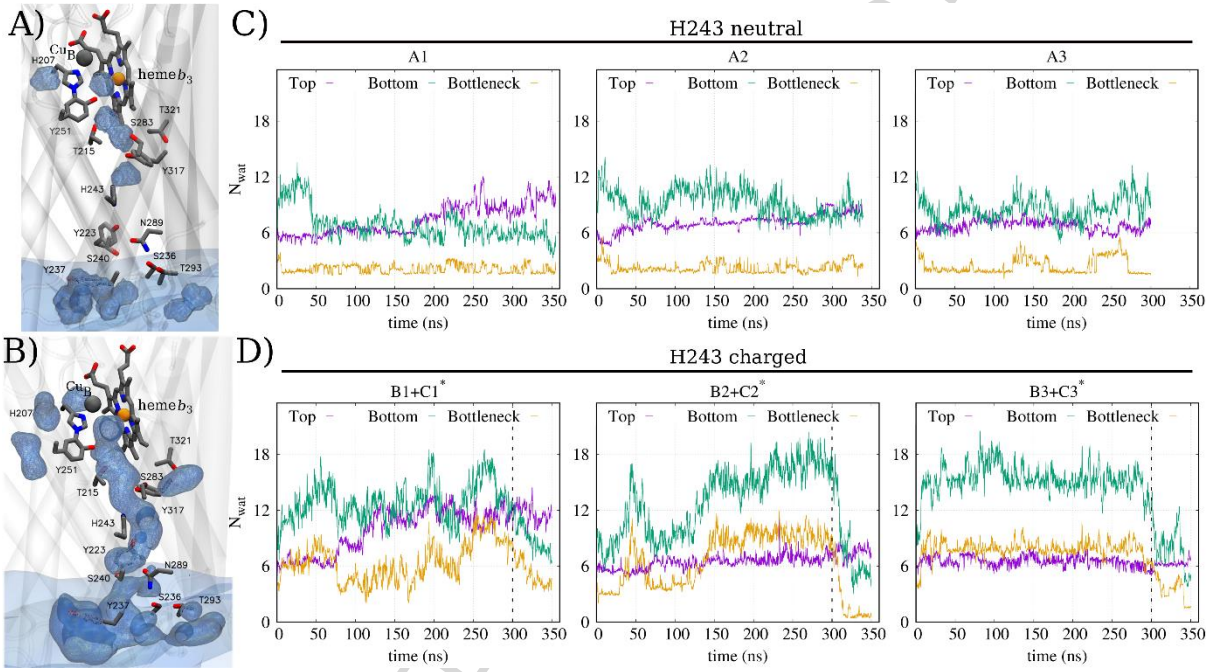


Figure 2. $K_c$-channel hydration depends on the protonation state of H243. **(A-B)** The water occupancy within 4Å of the $K_c$-channel residues and residues H207 and T321 is represented as a blue mesh for simulations A1, with H243 neutral **(A)**, and B1, with H243 charged **(B)**. Similar results are obtained for other replicas (see Figure S2). The bulk water is shown as a light blue surface and subunit CcoN is shown as a transparent grey cartoon. **(C-D)**. The number of water molecules within 3Å of residues in the three regions of the $K_c$-channel is shown for simulations A1-3 **(C)**, and B1-3/C1*-3* **(D)**. In **(D)** the vertical dashed lines at 300 ns represent the deprotonation of H243, and the number of waters beyond that point corresponds to the extended simulations with H243 neutral (C1*-3*).

To further validate the role of H243 in the hydration of the $K_c$-channel, we changed its protonation state at the end of simulations B1-3 (at 300 ns) and extended the simulations – now with H243 neutral (simulations C1*-3*). Upon H243 neutralisation, in all simulations we observed a disruption of a continuous water chain and a significant decrease in the number of waters in the bottom part of the $K_c$-channel – to the level comparable to simulations A1-3 (Figure 2C and D). This confirms that the hydration of the $K_c$-channel is strongly influenced by the protonation state of H243, with a positive charge at position 243 facilitating the formation of a continuous internal water network. Also, the role of H243 in stabilizing the nearby water chains was suggested in one of the previous computational studies [41].

The importance of H243 for the $K_c$-channel hydration is not surprising given its location and the fact that no other ionisable residues are present in the bottleneck region. However, this residue is not conserved in all known *cbb*$_3$ oxidases [10], e.g. it is replaced by alanine in the majority of the *Campylobacterales* [12,18] and by serine in *Helicobacter* [18,64]. This shows that presence of a titratable residue at this position is not essential for the proton uptake in several species. The results from mutagenesis experiments of *cbb*$_3$s in which His is conserved also do not offer a straightforward interpretation: while the H243V variant in *Bradyrhizobium japonicum* [65] and *Rhodobacter capsulatus* [20] and the H243G variant in *Vibrio cholerae* [17] and *Rhodobacter sphaeroides* [18] exhibited lowered catalytic activity, the H243A variant of *R. sphaeroides* retained WT activity [66].

In order to understand the effect of a substitution by a small non-titratable residue at this position, we performed simulations for the H243G mutant. This mutation resulted in a more hydrated bottleneck region, in comparison with simulations A1-3 (Figure S3A); however a gap between G243 and the entrance of the $K_c$-channel is still present in both replicas (Figure S3B). This might explain a low activity observed for the H243G variants of *V. cholerae* [17] and *R. sphaeroides* [18], and suggests that presence of a histidine residue at this position is important. Also, this data confirms that presence of a small residue at this position provides additional space for accommodating extra water molecules, which might be important for species where H243 is not conserved.

### 3.2. Formation of the water channel and $K_c$-channel entrance

To gain mechanistic details of the formation of the water connectivity between the cytoplasm and the active site, the conformational dynamics in the $K_c$-channel was analysed in simulations exhibiting a continuous water channel (B1-3, with H243 charged). Overall, subunit CcoN remains stable throughout our simulations, and no significant displacement of the transmembrane helices lining the $K_c$-channel (namely helices α6, α7, α8, and α9) is observed upon the water channel formation (rmsd remained below ~1.5Å, data not shown). This suggests that the event involves rearrangement of sidechains, and next we focus on the conformational dynamics of individual residues. Although there are variations to the mechanism, we identified several possible scenarios, with the common feature that the conformational changes of two polar residues located below H243, namely N289 and Y223, are always associated with the formation of the water chains in the $K_c$-channel bottleneck. Figure 3 presents the data (rmsd values and pair-wise distances) that characterise the conformational changes of these residues, along with the number of water molecules in the

region. The representative MD snapshots illustrating the conformational changes and dynamic of water chains are shown in Figure 3C and Figure S4. In simulation B1, the initial increase in the number of water molecules in the bottleneck region correlates with the displacement of the sidechains of N289 and Y223 (Figure 3A). This local structural reorientation leads to the formation of a persistent H-bond interaction between N289 and Y223, which then blocks the water connection to the top part of the $K_c$-channel until 250 ns, when a new sidechain reorientation is observed (Figure 3B and 3C and Figure S4). Interestingly, while the water connection between these two residues is disrupted, an alternative route is observed around Y223 and bypassing H243 (Figure S4). In simulation B2, the initial increase in the number of waters in the bottleneck region (at 45-50 ns) correlates with the Y223 sidechain displacement and disruption of the Y223-S240 and N289-H243 interactions (Figure 3). The subsequent gradual increase coincides with a displacement of the N289 sidechain, which moves away from Y223 at around 125 ns. This leads to a continuous water chain forming in the space between Y223, H243 and N289 (Figure S4). Finally, in simulation B3, there is an immediate increase in the number of water molecules in the bottleneck region; this number then remains constant until the end of the simulation (Figure 3). The water chain formation correlates with the Y223 sidechain reorientation and disruption of the H-bond interactions with S240 and N289. In turn, the sidechain of N289 gradually rotates and moves away from T293. In this simulation the forming water chain bypasses the polar cluster region below H243 and most of the time is bridged to the top part of the $K_c$-channel by the H243 imidazole ring (Figure S4). In summary, although we observe slight changes in terms of the local structural rearrangements associated with the formation of a continuous water channel, the reorientation of the sidechain of Y223 and N289 is common to all cases. Upon H243 deprotonation (in simulations C1*-3*), reorientation of these two residues correlates with the decrease in the number of waters located at the bottleneck region (Figure 3A and 3B). This finding is consistent with previous experimental observations. It was shown that mutations of the residues equivalent to N289 and Y223 in *Vibrio cholera*, *Rhodobacter capsulatus* and *Rhodobacter sphaeroides* $cbb_3$ lead to impaired activity, most likely due to blockage/disruption of the proton pathway [17,18,21].

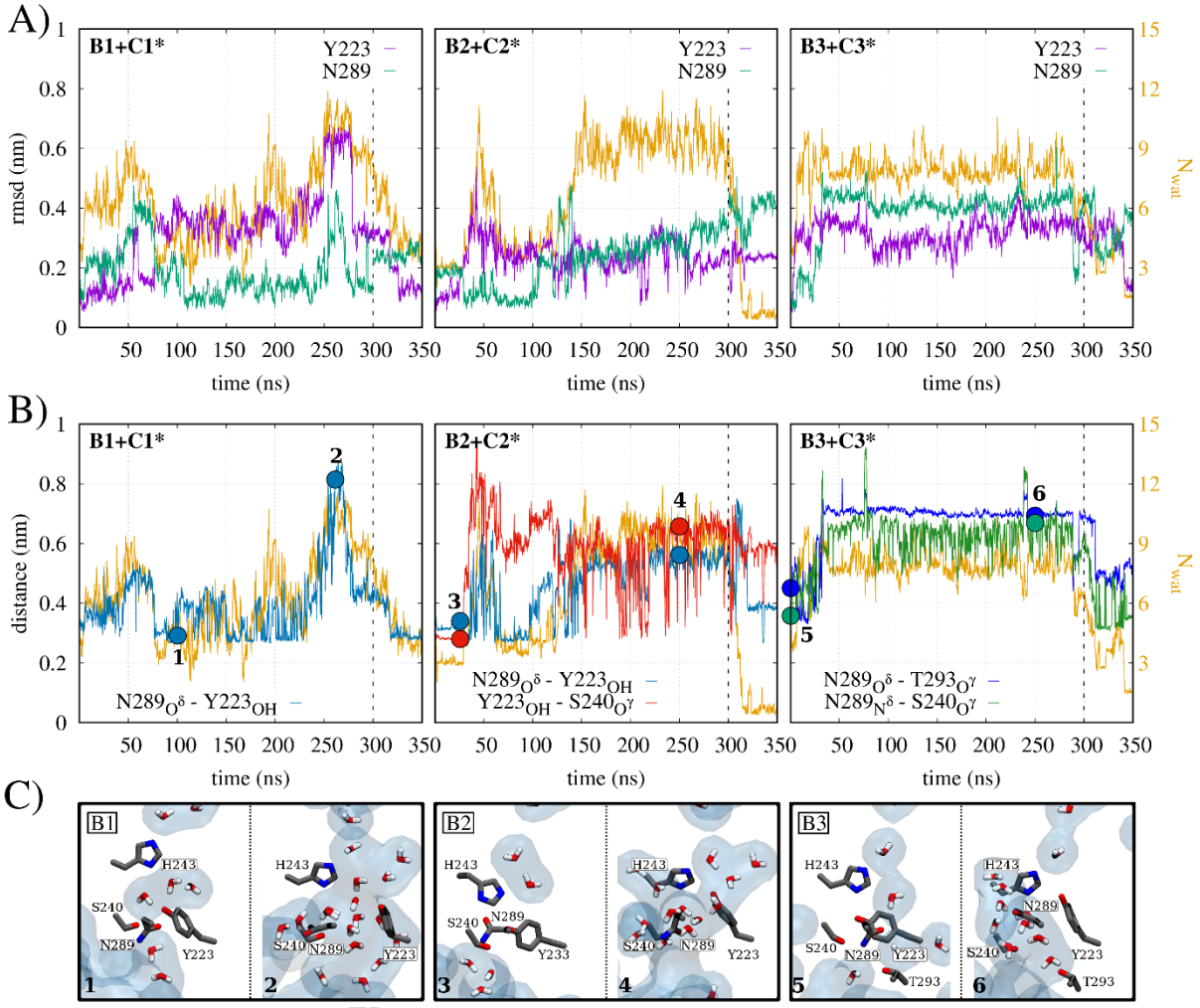


Figure 3. Conformational rearrangements associated with the formation of a continuous water channel in the $K_c$-channel. **(A)** Rmsd of sidechains of the residues Y233 (violet line) and N289 (green) and the number of waters in the bottleneck part (orange line) in simulations B1+C1* (left), B2+C2* (middle) and B3+C3* (right). **(B)** Distances between the polar residues which are involved in the water channel formation in each simulation: N289-Y233 in B1+C1*; N289-Y233 and Y223-S240 in B2+C2*; N289-T293 and N289-S240 in B3+C3*. The numbered colour dots correspond to the MD snapshots shown in panel **(C). C)** Representative MD snapshots from simulations B1-3 illustrating dynamic water chains and formation of the water channel in the bottleneck region. For each simulation two snapshots are shown; more snapshots can be found in Figure S4. The water molecules are shown as sticks and using a surface representation (transparent blue). The vertical dashed lines in **(A)** and **(B)** at 300 ns represent the deprotonation of H243 and a starting point of simulations C1*-3*.

Previously, based on the results of MD simulations, Ahn *et al.* discussed an opening/closing mechanism in which the residue Y237, which is located close to the channel entrance (Figure 1E), acts as a gate controlling the water access to the $K_c$-channel. Three different conformations of Y237 – the so called "open-in", "open-out" and "closed" conformations – were observed in their simulations [17]. This mechanism is governed by sidechain conformations of Y237 and $E49^P$. In the "open" conformations, the orientation of the Y237 sidechain enables the formation of a continuous hydrated pathway from the bulk to the polar cluster in the bottom part of the $K_c$-channel. Such water chain is disrupted in the "close" conformation, when Y237 moves upwards towards V159, while $E49^P$ moves downwards

towards the bulk and away from S240. The authors suggested that this mechanism resembles the one observed at the entrance of the D-channel in the A-type oxidases. We carried out similar analysis and found that this mechanism is not confirmed by our simulations B1-3 (Figure S5B). We did observe the conformations discussed by Ahn. *et al.*, however there is no correlation between the orientation of the sidechain of Y237 and variations in the number of waters at the entrance (i.e. bottom part) of the $K_c$-channel. Also, there is no correlation between the $E49^P$ "up" or "down" conformations and the number of waters in this region (Figure S5B). It should be noted that the number of waters populating this region was much lower in the simulations by Ahn *et al.* (up to 5 water molecules) in comparison with our study (up to 20 water molecules, Figure 2D); this could explain the discrepancy between the scenarios observed in the two works. This difference could also be due to the fact that H243 was treated in the neutral (deprotonated) state in the study by Ahn *et al.* Nevertheless, our analysis of the simulations with H243 neutral (A1-3, see Figure S5A) still does not reveal a correlation between Y237 orientation and the hydration of the channel entrance.

Finally, analysis of the entrance of the $K_c$-channel identified two main plausible proton uptake routes from the bulk. The first proceeds as $E8^O \rightarrow$ Y237 $\rightarrow E49^P$, while the second involves residues $E48^P$ and $E49^P$ (Figure 4). These two pathways are well illustrated by the water occupancy distributions in all simulations; similar results are observed in simulations A1-3 (data not shown). It should be noted that upon formation of the water connections, the solvent-exposed N-terminal region of subunit CcoP is displaced in all simulations (Figure S6). Interestingly, an alternative pathway leading directly to the bottleneck region in the $K_c$-channel was observed in simulation B3; this involves residues $N52^P \rightarrow$ Y235 $\rightarrow$ N289 $\rightarrow$ H243 (Figure 4, right), and might be a consequence of a partial blockage of the $E48^P \rightarrow E49^P$ route in this case. We conclude that $E49^P$ is the key residue involved in the proton uptake pathways from the cytoplasm (Figure 4). This is in agreement with the experimental results which confirmed the role of this residue as the entry point to the proton pathway in *Rhodobacter sphaeroides* $cbb_3$ [22] and *Vibrio cholera* $cbb_3$ [17]. The mutations $E49^P$A/Q (*P. stutzeri* numbering) were experimentally shown to severely impair the oxidase activity [17,22], while the mutation $E49^P$K reduced the wild-type (WT) activity by half [22], and $E49^P$D retained the WT activity [17].

In order to further understand the importance of $E49^P$ for the proton uptake, we performed simulations for the $E49^P$A mutant (with H243 in the charged state). In these simulations, the entrance region of the $K_c$-channel was significantly less hydrated (Figure S7) in comparison

with the results obtained in simulations B1-3 (Figure 2D and Figure 4). The number of water molecules in the bottom and bottleneck regions of the $K_c$-channel (around 6-7 and 3-4, respectively) was comparable to that observed in simulations A1-3 (compare plots in Figure S7A and Figure 2C). Also, the main proton uptake pathways shown in Figure 4 are affected in the E49A$^P$ variant. Interestingly, the neighbour glutamate, E48$^P$, does not take up the role of the mutated E49$^P$, remaining fully extended to the bulk as observed in the WT simulations (data not shown). This shows that the presence of a titratable residue at position 49 is essential for the (proton uptake and) enzymatic activity, and highlights the preference for a negatively charged residue. The role of E8$^O$ in proton uptake was ruled out after the E8$^O$A/Q mutants exhibited WT activities [17]. Together with our observations, these results suggest that even with the E8$^O$ → Y237 → E49$^P$ pathway blocked, the proton uptake to the $K_c$-channel can proceed via the E48$^P$ → E49$^P$ route. This hypothesis can be verified experimentally by making a mutant in which both main water/proton intake routes are blocked, such as e.g. the double mutant E8$^O$A/E48$^P$A.

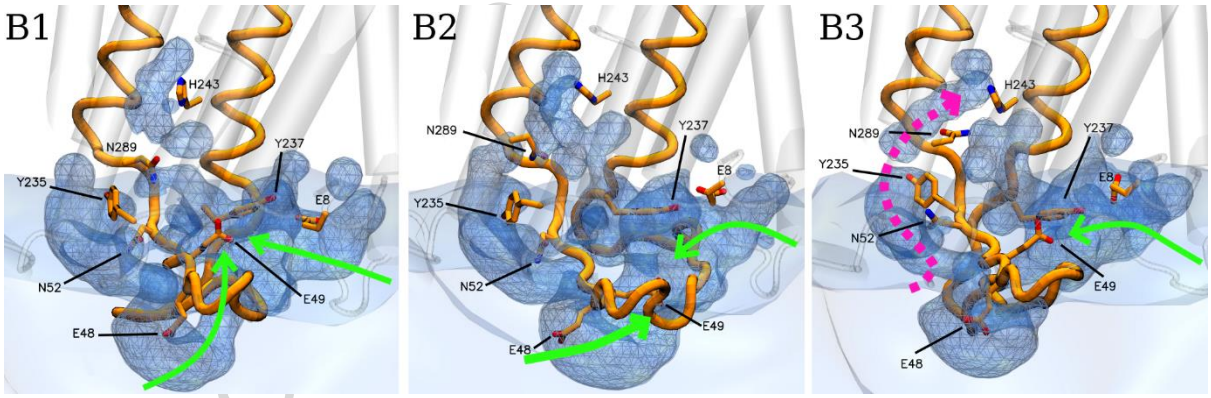


Figure 4. $K_c$-channel entrance region. Water occupancy within 4 Å of polar residues in the region (Y223, Y235, S236, Y237, S240, H243, N289, T293, E8$^O$, E48$^P$, E49$^P$ and N52$^P$) in simulations B1-3 is represented as a blue mesh. The plausible proton uptake pathways are indicated by green arrows, and an alternative proton uptake pathway, observed in simulation B3, is shown in magenta. Relevant residues are shown as sticks. Subunit CcoP is shown in orange, and subunits CcoN and CcoO are shown as a transparent cartoon. The bulk water is shown as a light blue surface.

## 3.3. Proton exit pathway and gating mechanism

### *3.3.1. E323 and H337 are part of the PLS*

Since in *cbb*$_3$ there is only one proton pathway from the cytoplasmic side, the chemical and pumped protons must share it up to some point in the top part of the $K_c$-channel, after which they will diverge. Then, for the pumped protons there must be a further pathway to the water-filled hydrophilic cavity, which is connected to the periplasmic side of the membrane. Such pathway should involve a redox-controlled gating mechanism and PLS. Sharma *et al* [41] proposed a plausible pathway that leads from Y317 at the top of $K_c$-channel along the

residues T321, S320, E323 "behind" the active site heme to H337 and A-propionate of heme $b_3$. It should be noted that E323 is positioned far away from both the top part of $K_c$-channel (~13 Å to Y317) and the cluster above heme $b_3$ (~14 Å to H337). Therefore it is expected that transiently forming water chains will bridge the gaps and provide a pathway for proton translocation. We investigated the water dynamics in this region, including the effect of the protonation state of H337 and E323. In simulations A, B and C both residues were simulated in the charged state ($His^+$, $Glu^-$). No water connections were observed between E323 and H337 or Y317 in either of these simulations, so the proton translocation is blocked in this configuration. Importantly, a stable salt-bridge interaction is maintained between H337 and the A-propionate of heme $b_3$ in all cases (Figure 5A). The effect of the protonation state of H337 and E323 was studied by extending the simulations B1-3 after neutralising H337 or E323 – simulations D1*-3* and E1*-2*, respectively.

Upon neutralisation of H337 (simulations D1*-3*) a previously stable salt-bridge between H337 and A-propionate is broken and the sidechain of H243 moves away (Figure 5A). At the same time, the number of water molecules around E323 increases from 2-5 to 7-8 (Figure 5A), and this in turn disrupts the labile H-bond interaction between E323 and H345 (Figure 5A). These local structural events facilitate formation of a stable water connection between E323 and the A-propionate in all three simulations, as illustrated in Figure 5B. Furthermore, in simulation D1* the increase in the E323 hydration is accompanied by a local displacement of helix α9 (Figure S8) and rearrangement of the sidechains of Y317, S320, T321 and M327 (Figure 5C). These changes together facilitate formation of a water connection between E323 and Y317 (Figure 5B), thus providing a continuous pathway for proton translocation from Y317 to H337/A-propionate. Interestingly, the H-bond between E323 and H345 is recovered and stabilized upon the formation of this pathway in simulation D1* (Figure 5A). No such structural changes were observed in the two other simulations (D2* and D3*), which prevented the water connection between E323 and Y317 (Figure 5B and 5C and Figure S8). These observations suggest that local structural rearrangements (helix and/or sidechains), which open space for water molecules, are required for the formation of protonic connections along the pumping pathway, and they can be triggered by the H337 neutralisation and dissociation from A-propionate.

Neutralisation of E323 (simulations E1*-3*) greatly reduced its local hydration (Figure S9A), which precludes formation of the proton exit pathways observed upon H337 neutralisation (compare Figure S9B and Figure 5B). Interestingly, this had a stabilising effect on the H-

bond interaction between E323 and H435 (Figure S9A). These observations suggest that the protonation state of E323 greatly affects the local hydration and stability of its H-bond connectivity to H345.

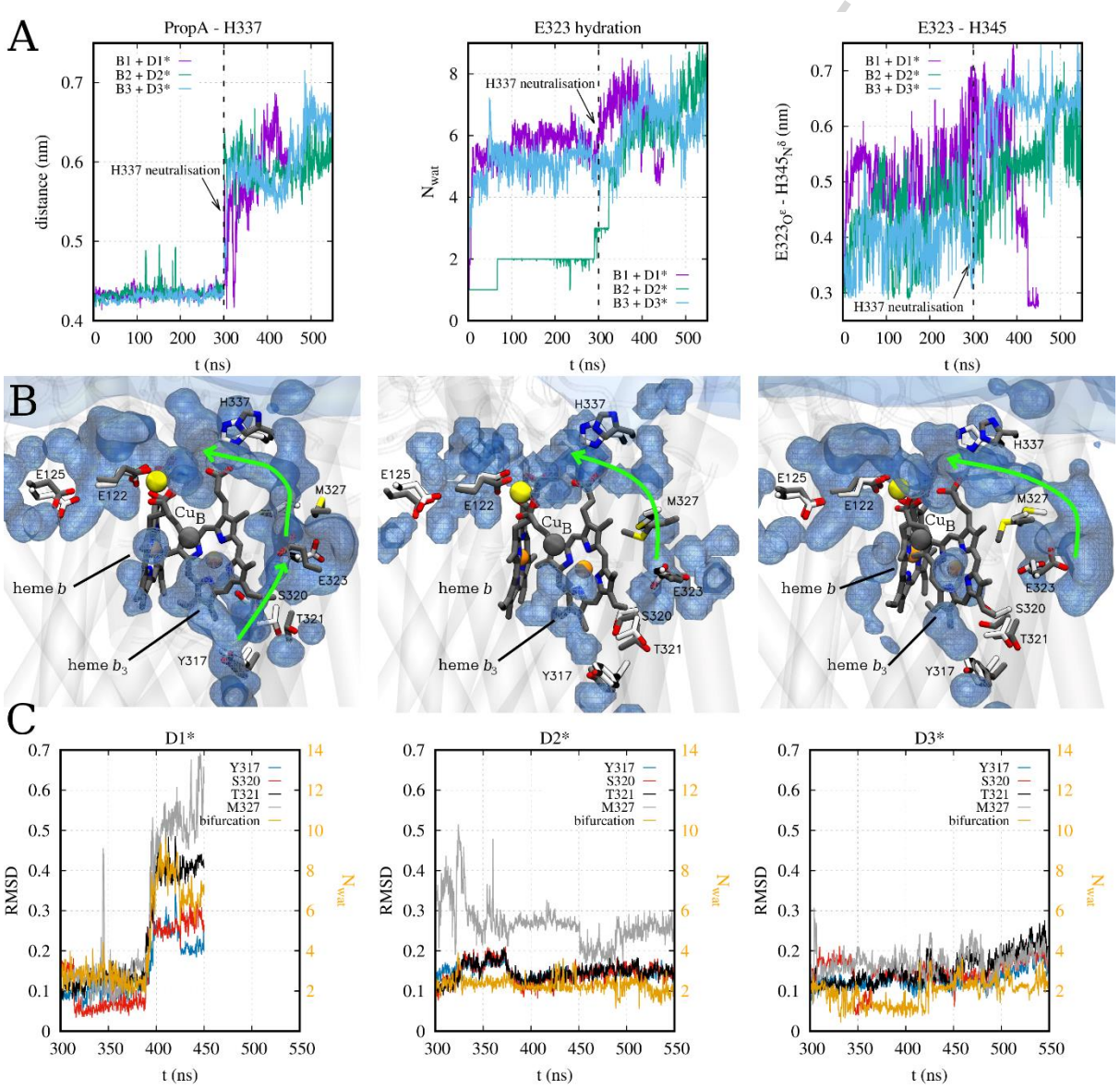


Figure 5. Proton pumping and exit pathways. **(A)** Distance between the C atom of the carboxyl group of the A-propionate of heme $b_3$ and imidazole ring of H377 (left), number of waters within 3 Å of E323 (middle), and distance between the sidechains of E323 and H345 (right) in simulations B1-3/D1*-3*. The vertical dashed line at 300 ns indicates neutralisation of H337 and starting point of simulations D1*-D3*. **(B)** Water occupancy within 4 Å of residues around BNC (namely, E122, E125, S320, E323, M327, H337, T339, W341, T342, H345, W400) is represented as a blue mesh for simulations D1*-3* (left, middle and right, respectively). The initial and final conformations of the highlighted residues are shown as white and grey sticks, respectively, the bulk water at the periplasmic side is shown as a light blue surface, and the calcium ion is shown as a yellow sphere. The plausible proton pathways are indicated by green arrows. **(C)** Rmsd of the sidechains of Y317, S320, T321 and M327, and number of waters within 3 Å of S320, T321 and H345 in simulations D1*-3*.

In order to test whether local conformational changes would affect the protonation equilibria of these two residues, we performed p$K_a$ calculations using a Poisson-Boltzmann/Monte Carlo approach for multiple snapshots sampled from each MD simulation. The results of the

p$K_a$ calculations for E323 and H337 are presented in Table 2. The p$K_a$ values obtained for E323 are in the range 5-6 in simulations A-D, in agreement with similar calculations by Sharma *et al.* [41]. This suggests that in this case E323 is likely to be titrating, and small changes in the local environment (e.g. hydration level or redox changes in the nearby heme $b_3$) could affect its protonation state. In simulations E, an upward shift of ~2-3 pKa units is observed, suggesting a stabilisation of the neutral state. As for H337, the p$K_a$ values obtained are >10 for all simulations, except for D1*-3*, where H337 exhibits a lower p$K_a$ value around ~6-7. This means that in all cases, except for D1*-3*, the charged (protonated) form of H337 is stabilised due to a strong salt-bridge interaction with the negatively charged A-propionate of heme $b_3$. In simulations D1*-3*, the lower p$K_a$ value is a consequence of a dissociation of the (deprotonated) imidazole ring of H337 from A-propionate; H337 is rather titrating in such conditions.

**Table 2.** Results of the p$K_a$ calculations for residues E323 and H337 in different simulation systems. The Poisson Boltzmann/Monte Carlo calculations were performed as described in Supplementary Material. Multiple snapshots ($N_{snaps}$) for p$K_a$ calculations were sampled from each MD simulation with a 5 ns interval. The average over all snapshots and standard deviation (SD) for each simulation are presented.

| Simulation | | $N_{snaps}$ | E323 | | H337 | |
|---|---|---|---|---|---|---|
| | | | p$K_a$ | SD | p$K_a$ | SD |
| A | 1 | 56 | 6.0 | 0.5 | 11.5 | 0.7 |
| | 2 | | 5.7 | 0.4 | 12.2 | 0.4 |
| | 3 | | 5.9 | 0.5 | 11.8 | 0.4 |
| B | 1 | 56 | 5.6 | 0.5 | 12.4 | 0.5 |
| | 2 | | 5.7 | 0.6 | 12.3 | 0.4 |
| | 3 | | 5.7 | 0.5 | 12.3 | 0.5 |
| C | 1* | 10 | 5.6 | 0.4 | 11.9 | 0.5 |
| | 2* | | 6.2 | 0.3 | 12.1 | 0.4 |
| | 3* | | 6.1 | 0.4 | 12.0 | 0.4 |
| D | 1* | 30 | 5.1 | 0.6 | 7.0 | 1.4 |
| | 2* | | 5.4 | 0.6 | 6.7 | 0.7 |
| | 3* | | 5.7 | 0.6 | 6.0 | 0.9 |
| E | 1* | 20 | 8.6 | 0.7 | 12.4 | 0.4 |
| | 2* | | 8.6 | 0.5 | 12.5 | 0.5 |
| | 3* | | 8.2 | 0.5 | 12.0 | 0.4 |

Assuming a scenario where redox changes in the BNC during the catalytic cycle stabilise a neutral state of H337 and a charged state of E323, this would lead to an increase of E323 hydration and facilitate the formation a water connectivity between Y317 and the A-propionate of heme $b_3$, thus providing a pathway for the pumped proton towards the periplasmic side of the membrane (Figure 5). This pathway is similar to the one observed in

MD simulations by Sharma *et al.* [41]. Our observations suggest that formation of such proton exit pathway is controlled by the protonation state of H337 and E323 and involves local conformational changes of the residues Y317, S320, T321 and M327.

*3.3.2. Y317 is a bifurcation point*

Y317 was previously suggested to serve as a bifurcation point in $cbb_3$ [21,41]. This proposal is in tune with our results of simulation D1*, which showed that pathways for the chemical and pumped protons diverge at this point (see Figure 5B and discussion therein).

In *Rhodobacter capsulatus*, the T215A variant was shown to decouple oxygen reduction from proton pumping resulting only in a decrease of the pumping activity (~ 20% of the WT) [21]. This suggested that such mutation would affect the branching point (Y317) in a way that the proton translocation towards the outer side of the membrane is no longer possible. Furthermore, a mutation of the residue Y317 to a phenylalanine was shown impair $cbb_3$'s enzymatic activity in *Vibrio cholerae* [18] and *Rhodobacter capsulatus* [21], which precluded the understanding of the impact of such mutation on the proton pumping activity.

In order to investigate the effect of such mutations in the bifurcation region, we performed simulations for the T215A and Y317F variants. The results for T215A are rather inconclusive, as this mutation only resulted in a slight decrease of the number of waters in the bottom part of the $K_c$-channel (in agreement with previous observations [17,18]), and had no effect on the pre-formed exit pathway (Figure S10). The Y317F mutant exhibited significant dehydration towards the BNC, but at the same time increased hydration in the bifurcation region between F317 with E323 (Figure S11). In one replica the exit proton pathway observed in simulation D1* was also present. Therefore, along with affecting the water connection to the active site, this mutation seems to change the water preference towards the pumping route, enabling access via E323.

Altogether, our results emphasize the role of Y317 in controlling the proton pathways from the $K_c$-channel to either the active site or the periplasmic side of the membrane.

*3.3.3. Redox-controlled proton pumping mechanism*

Despite the distinct functional and structural features of C-type oxidases, similar principles are expected to govern the coupling mechanism between the chemical reaction and proton pumping in all oxidases [2–4,23]. The consequence of redox-induced local structural changes on specific reaction steps that are rate limiting for proton pumping, was recently demonstrated for an A-type oxidase [23]. Moreover, mutations in residues "above" the active

site were shown to uncouple the enzymatic activity from the proton pumping activity in a B-type oxidase, possibly by preventing protonation of the PLS [38] located in this region [40]. This was further validated by recent computational studies [39,67,68], in which H376 in *Thermus thermophilus* $ba_3$, which sits at a position equivalent to H337 in $cbb_3$ and interacts with the A-propionate of the active site heme, was identified as part of the PLS. Given a closer structural relation between the B- and C-families [7,26], in particular presence of a single proton channel, and the results presented here, it is likely that the proton exit pathway and the PLS are similar in these two families. Based on this assumption, we propose a redox-driven pumping mechanism for $cbb_3$. Initially, the pumping route is closed and the positively charged H337 forms a salt-bridge with the propionate A of heme $b_3$. The redox changes in the active site (possibly heme $b_3$ oxidation) shift the p$K_a$ of H337 down and stabilise its neutral form; H337 donates a proton towards the periplasm and dissociates from A-propionate, enabling formation of a continuous water connectivity between the $K_c$-channel and the hydrophilic region above the active site. A proton is then translocated along this pathway via E323 to H337. The transient protonation of E323 leads to local changes, which will close the water connection between Y317 and E323, ensuring the unidirectional proton translocation towards H337. H337 is eventually (re)protonated, and the pumping route is closed until the next pumping step in the catalytic cycle. To test this plausible proton exit pathway, we propose to mutate H337 to a non-titratable residue, e.g. asparagine. Another option is to replace M327 by a bulky nonpolar residue, e.g. phenylalanine or tryptophan. We expect these to be uncoupling mutants, i.e. they will affect the pumping efficiency without decreasing the catalytic activity.

It is noteworthy that in our simulations no water connections were observed between the active site and residues E125 and E122 (Figure 5B), thus excluding the possibility of a proton exit pathway involving these residues [10]. A potential connection between the active site and E122 is blocked by the calcium ion and Y123; the latter residue maintains a persistent hydrogen bond interaction with the D-propionate of heme $b_3$ (Figure S12).

## 4. Conclusions

In this work we used molecular dynamics simulations (in total ~4.6 μs) together with continuum electrostatic calculations to obtain the atomic-level details of internal water

dynamics and proton transfer pathways in cytochrome *cbb*$_3$ oxidase. We have established that the K$_c$-channel has a bottleneck region around H243 and that the channel hydration is highly influenced by the protonation state of this residue – only simulations with the charged H243 consistently displayed formation of a continuous and stable water channel in the bottleneck region of the K$_c$-channel. It must be noted that since this residue is not fully conserved in *cbb*$_3$ oxidases, its role in the proton transfer through the K$_c$-channel requires more studies. We also shown that sidechain conformational changes of Y223 and N289 are associated with the mechanistic formation of a continuous water channel through the bottleneck region. E49$^P$ in the entrance region of the K$_c$-channel has been confirmed as the key residue participating in the uptake of protons from the bulk. All these findings are consistent with the high conservation of the identified key residues and previously reported mutagenesis data.

In light of observations from MD simulations and p$K_a$ calculations, we have proposed a redox-driven pumping mechanism, in which H337 and E323 participate in the exit pathway and likely act as PLS. The (redox triggered) neutralisation of H337 (and release of a proton towards periplasm) primes local conformational changes, which lead to the formation of a continuous water connection, and a plausible proton pumping route, between the top part of K$_c$-channel (Y317, the suggested bifurcation point) and hydrophilic region above heme $b_3$. A proton is then transferred via E323 to H377, which is reprotonated, and the transient pathway is closed, ensuring the unidirectional proton translocation. We observed that in the Y317F mutant the water connectivity to the BNC is disrupted, while hydration of the bifurcation region increases. This emphasises the role of Y317 as the branching.

It should be noted that the methods used in this work, namely classical MD simulations and continuum electrostatics calculations, cannot in principle describe the actual proton transfer processes. Our results provide the information about plausible proton pathways, key residues involved in and conditions required for formation of protonic connections; details of the explicit proton translocation are out of the scope of this work and will be the focus of future publications. Also, the effect of different redox states, corresponding to various intermediates of the catalytic cycle, is not addressed here and will be explored in the subsequent papers. Our preliminary data suggests that some of the events described in this work (changes of the protonation equilibria of key residues) could be achieved by redox changes in the metal centres.

This work provides new insights into the proton pathways in *cbb*$_3$ oxidase and offers a basis for future experimental and computational studies. In particular, based on our results we have proposed three mutations which can be tested experimentally to confirm the details of the proton pathways and mechanism: the double mutant E8$^{O}$A/E48$^{P}$A would clarify the role of these two residues in the proton uptake from the cytoplasm, while the M327F/W and H337N mutants would possibly confirm the pumping route and role of H337 as part of the PLS.

## Acknowledgements

This work was funded by the Scottish Universities Physics Alliance (SUPA). We also appreciate support from the University of Dundee Life Sciences Computing cluster. Access to ARCHER National Supercomputing Service was provided through the HEC-Biosim Consortium.

# References

[1] H.J. Lee, E. Svahn, J.M.J. Swanson, H. Lepp, G.A. Voth, P. Brzezinski, R.B. Gennis, Intricate role of water in proton transport through cytochrome c oxidase, J. Am. Chem. Soc. 132 (2010) 16225–16239. doi:10.1021/ja107244g.

[2] M. Wikström, V. Sharma, V.R.I. Kaila, J.P. Hosler, G. Hummer, New Perspectives on Proton Pumping in Cellular Respiration, Chem. Rev. 115 (2015) 2196–2221. doi:10.1021/cr500448t.

[3] S. Yoshikawa, A. Shimada, Reaction Mechanism of Cytochrome c Oxidase, Chem. Rev. 115 (2015) 1936–1989. doi:10.1021/cr500266a.

[4] S. Ferguson-Miller, C. Hiser, J. Liu, Gating and regulation of the cytochrome c oxidase proton pump, Biochim. Biophys. Acta BBA - Bioenerg. 1817 (2012) 489–494. doi:10.1016/j.bbabio.2011.11.018.

[5] M.M. Pereira, M. Santana, M. Teixeira, A novel scenario for the evolution of haem-copper oxygen reductases, Biochim. Biophys. Acta. 1505 (2001) 185–208.

[6] F.L. Sousa, R.J. Alves, J.B. Pereira-Leal, M. Teixeira, M.M. Pereira, A Bioinformatics Classifier and Database for Heme-Copper Oxygen Reductases, PLoS ONE. 6 (2011) e19117. doi:10.1371/journal.pone.0019117.

[7] F.L. Sousa, R.J. Alves, M.A. Ribeiro, J.B. Pereira-Leal, M. Teixeira, M.M. Pereira, The superfamily of heme–copper oxygen reductases: Types and evolutionary considerations, Biochim. Biophys. Acta BBA - Bioenerg. 1817 (2012) 629–637. doi:10.1016/j.bbabio.2011.09.020.

[8] R.S. Pitcher, N.J. Watmough, The bacterial cytochrome cbb3 oxidases, Biochim. Biophys. Acta BBA - Bioenerg. 1655 (2004) 388–399. doi:10.1016/j.bbabio.2003.09.017.

[9] Y. Huang, J. Reimann, L.M.R. Singh, P. Ädelroth, Substrate binding and the catalytic reactions in cbb3-type oxidases: The lipid membrane modulates ligand binding, Biochim. Biophys. Acta BBA - Bioenerg. 1797 (2010) 724–731. doi:10.1016/j.bbabio.2010.03.016.

[10] S. Buschmann, E. Warkentin, H. Xie, J.D. Langer, U. Ermler, H. Michel, The structure of cbb3 cytochrome oxidase provides insights into proton pumping, Science. 329 (2010) 327–330. doi:10.1126/science.1187303.

[11] M. Kohlstaedt, S. Buschmann, H. Xie, A. Resemann, E. Warkentin, J.D. Langer, H. Michel, Identification and Characterization of the Novel Subunit CcoM in the cbb3-Cytochrome c Oxidase from Pseudomonas stutzeri ZoBell, mBio. 7 (2016). doi:10.1128/mBio.01921-15.

[12] V. Sharma, A. Puustinen, M. Wikström, L. Laakkonen, Sequence Analysis of the cbb3 Oxidases and an Atomic Model for the Rhodobacter sphaeroides Enzyme†, Biochemistry (Mosc.). 45 (2006) 5754–5765. doi:10.1021/bi060169a.

[13] T. Hino, Y. Matsumoto, S. Nagano, H. Sugimoto, Y. Fukumori, T. Murata, S. Iwata, Y. Shiro, Structural Basis of Biological N2O Generation by Bacterial Nitric Oxide Reductase, Science. 330 (2010) 1666–1670. doi:10.1126/science.1195591.

[14] Y. Matsumoto, T. Tosha, A.V. Pisliakov, T. Hino, H. Sugimoto, S. Nagano, Y. Sugita, Y. Shiro, Crystal structure of quinol-dependent nitric oxide reductase from Geobacillus stearothermophilus, Nat. Struct. Mol. Biol. 19 (2012) 238–245. doi:10.1038/nsmb.2213.

[15] N. Agmon, The Grotthuss mechanism, Chem. Phys. Lett. 244 (1995) 456–462. doi:10.1016/0009-2614(95)00905-J.

[16] Y.Y. Sham, I. Muegge, A. Warshel, Simulating proton translocations in proteins: probing proton transfer pathways in the Rhodobacter sphaeroides reaction center, Proteins. 36 (1999) 484–500.

[17] Y.O. Ahn, P. Mahinthichaichan, H.J. Lee, H. Ouyang, D. Kaluka, S.-R. Yeh, D. Arjona, D.L. Rousseau, E. Tajkhorshid, P. Adelroth, R.B. Gennis, Conformational coupling between the active site and residues within the K(C)-channel of the Vibrio cholerae cbb3-type (C-family) oxygen reductase, Proc. Natl. Acad. Sci. U. S. A. 111 (2014) E4419-4428. doi:10.1073/pnas.1411676111.

[18] J. Hemp, H. Han, J.H. Roh, S. Kaplan, T.J. Martinez, R.B. Gennis, Comparative Genomics and Site-Directed Mutagenesis Support the Existence of Only One Input Channel for Protons in the C-Family (cbb3 Oxidase) of Heme−Copper Oxygen Reductases†, Biochemistry (Mosc.). 46 (2007) 9963–9972. doi:10.1021/bi700659y.

[19] M. Öztürk, S. Mandaci, Two conserved non-canonical histidines are essential for activity of the cbb 3-type oxidase in Rhodobacter capsulatus, Mol. Biol. Rep. 34 (2006) 165–172. doi:10.1007/s11033-006-9031-9.

[20] M. Ozturk, E. Gurel, N.J. Watmough, S. Mandaci, Site-directed mutagenesis of five conserved residues of subunit i of the cytochrome cbb3 oxidase in Rhodobacter capsulatus, J. Biochem. Mol. Biol. 40 (2007) 697–707.

[21] G.G. Yıldız, R.B. Gennis, F. Daldal, M. Öztürk, The KC Channel in the cbb3-Type Respiratory Oxygen Reductase from Rhodobacter capsulatus Is Required for Both Chemical and Pumped Protons, J. Bacteriol. 196 (2014) 1825–1832. doi:10.1128/JB.00005-14.

[22] H.J. Lee, R.B. Gennis, P. Ädelroth, Entrance of the proton pathway in cbb3-type heme-copper oxidases, Proc. Natl. Acad. Sci. 108 (2011) 17661–17666. doi:10.1073/pnas.1107543108.

[23] J. Vilhjálmsdóttir, A.-L. Johansson, P. Brzezinski, Structural Changes and Proton Transfer in Cytochrome c Oxidase, Sci. Rep. 5 (2015) 12047. doi:10.1038/srep12047.

[24] I. Belevich, D.A. Bloch, N. Belevich, M. Wikström, M.I. Verkhovsky, Exploring the proton pump mechanism of cytochrome c oxidase in real time, Proc. Natl. Acad. Sci. 104 (2007) 2685–2690. doi:10.1073/pnas.0608794104.

[25] P. Goyal, J. Lu, S. Yang, M.R. Gunner, Q. Cui, Changing hydration level in an internal cavity modulates the proton affinity of a key glutamate in cytochrome c oxidase, Proc. Natl. Acad. Sci. 110 (2013) 18886–18891. doi:10.1073/pnas.1313908110.

[26] V.R.I. Kaila, V. Sharma, M. Wikström, The identity of the transient proton loading site of the proton-pumping mechanism of cytochrome c oxidase, Biochim. Biophys. Acta BBA - Bioenerg. 1807 (2011) 80–84. doi:10.1016/j.bbabio.2010.08.014.

[27] J. Lu, M.R. Gunner, Characterizing the proton loading site in cytochrome c oxidase, Proc. Natl. Acad. Sci. 111 (2014) 12414–12419. doi:10.1073/pnas.1407187111.

[28] A.V. Pisliakov, P.K. Sharma, Z.T. Chu, M. Haranczyk, A. Warshel, Electrostatic basis for the unidirectionality of the primary proton transfer in cytochrome c oxidase, Proc. Natl. Acad. Sci. 105 (2008) 7726–7731. doi:10.1073/pnas.0800580105.

[29] R. Sugitani, E.S. Medvedev, A.A. Stuchebrukhov, Theoretical and computational analysis of the membrane potential generated by cytochrome c oxidase upon single electron injection into the enzyme, Biochim. Biophys. Acta. 1777 (2008) 1129–1139. doi:10.1016/j.bbabio.2008.05.006.

[30] M. Wikström, M.I. Verkhovsky, Mechanism and energetics of proton translocation by the respiratory heme-copper oxidases, Biochim. Biophys. Acta BBA - Bioenerg. 1767 (2007) 1200–1214. doi:10.1016/j.bbabio.2007.06.008.

[31] T. Yamashita, G.A. Voth, Insights into the mechanism of proton transport in cytochrome c oxidase, J. Am. Chem. Soc. 134 (2012) 1147–1152. doi:10.1021/ja209176e.

[32] A.S.F. Oliveira, S.R.R. Campos, A.M. Baptista, C.M. Soares, Coupling between protonation and conformation in cytochrome c oxidase: Insights from constant-pH MD simulations, Biochim. Biophys. Acta BBA - Bioenerg. 1857 (2016) 759–771. doi:10.1016/j.bbabio.2016.03.024.

[33] T. Soulimane, G. Buse, G.P. Bourenkov, H.D. Bartunik, R. Huber, M.E. Than, Structure and mechanism of the aberrant ba3-cytochrome c oxidase from Thermus thermophilus, EMBO J. 19 (2000) 1766–1776. doi:10.1093/emboj/19.8.1766.

[34] C. Koutsoupakis, T. Soulimane, C. Varotsis, Probing the Q-Proton Pathway of ba3-Cytochrome c Oxidase by Time-Resolved Fourier Transform Infrared Spectroscopy, Biophys. J. 86 (2004) 2438–2444. doi:10.1016/S0006-3495(04)74300-3.

[35] J.A. Fee, D.A. Case, L. Noodleman, Toward a chemical mechanism of proton pumping by the B-type cytochrome c oxidases: application of density functional theory to cytochrome ba3 of Thermus thermophilus, J. Am. Chem. Soc. 130 (2008) 15002–15021. doi:10.1021/ja803112w.

[36] H.-Y. Chang, J. Hemp, Y. Chen, J.A. Fee, R.B. Gennis, The cytochrome ba3 oxygen reductase from Thermus thermophilus uses a single input channel for proton delivery to the active site and for proton pumping, Proc. Natl. Acad. Sci. 106 (2009) 16169–16173. doi:10.1073/pnas.0905264106.

[37] H.-Y. Chang, S.K. Choi, A.S. Vakkasoglu, Y. Chen, J. Hemp, J.A. Fee, R.B. Gennis, Exploring the proton pump and exit pathway for pumped protons in cytochrome ba3 from Thermus thermophilus, Proc. Natl. Acad. Sci. 109 (2012) 5259–5264. doi:10.1073/pnas.1107345109.

[38] C. von Ballmoos, N. Gonska, P. Lachmann, R.B. Gennis, P. Ädelroth, P. Brzezinski, Mutation of a single residue in the ba3 oxidase specifically impairs protonation of the

pump site, Proc. Natl. Acad. Sci. U. S. A. 112 (2015) 3397–3402. doi:10.1073/pnas.1422434112.

[39] L. Yang, Å.A. Skjevik, W.-G. Han Du, L. Noodleman, R.C. Walker, A.W. Götz, Water exit pathways and proton pumping mechanism in B-type cytochrome c oxidase from molecular dynamics simulations, Biochim. Biophys. Acta BBA - Bioenerg. 1857 (2016) 1594–1606. doi:10.1016/j.bbabio.2016.06.005.

[40] A. Nicolaides, T. Soulimane, C. Varotsis, ns-μs Time-Resolved Step-Scan FTIR of ba3 Oxidoreductase from Thermus thermophilus: Protonic Connectivity of w941-w946-w927, Int. J. Mol. Sci. 17 (2016) 1657. doi:10.3390/ijms17101657.

[41] V. Sharma, M. Wikström, V.R.I. Kaila, Dynamic water networks in cytochrome cbb3 oxidase, Biochim. Biophys. Acta BBA - Bioenerg. 1817 (2012) 726–734. doi:10.1016/j.bbabio.2011.09.010.

[42] A.V. Pisliakov, T. Hino, Y. Shiro, Y. Sugita, Molecular Dynamics Simulations Reveal Proton Transfer Pathways in Cytochrome C-Dependent Nitric Oxide Reductase, PLOS Comput Biol. 8 (2012) e1002674. doi:10.1371/journal.pcbi.1002674.

[43] M.H.M. Olsson, P.K. Sharma, A. Warshel, Simulating redox coupled proton transfer in cytochrome c oxidase: Looking for the proton bottleneck, FEBS Lett. 579 (2005) 2026–2034. doi:10.1016/j.febslet.2005.02.051.

[44] J. Quenneville, D.M. Popović, A.A. Stuchebrukhov, Combined DFT and electrostatics study of the proton pumping mechanism in cytochrome c oxidase, Biochim. Biophys. Acta BBA - Bioenerg. 1757 (2006) 1035–1046. doi:10.1016/j.bbabio.2005.12.003.

[45] S. Chakrabarty, I. Namslauer, P. Brzezinski, A. Warshel, Exploration of the cytochrome c oxidase pathway puzzle and examination of the origin of elusive mutational effects, Biochim. Biophys. Acta BBA - Bioenerg. 1807 (2011) 413–426. doi:10.1016/j.bbabio.2011.01.004.

[46] P. Goyal, S. Yang, Q. Cui, Microscopic basis for kinetic gating in Cytochrome c oxidase: insights from QM/MM analysis, Chem. Sci. R. Soc. Chem. 2010. 6 (2015) 826–841. doi:10.1039/C4SC01674B.

[47] B.M. Samudio, V. Couch, A.A. Stuchebrukhov, Monte Carlo Simulations of Glu-242 in Cytochrome c Oxidase, J. Phys. Chem. B. 120 (2016) 2095–2105. doi:10.1021/acs.jpcb.5b10998.

[48] R. Liang, J.M.J. Swanson, Y. Peng, M. Wikström, G.A. Voth, Multiscale simulations reveal key features of the proton-pumping mechanism in cytochrome c oxidase, Proc. Natl. Acad. Sci. 113 (2016) 7420–7425. doi:10.1073/pnas.1601982113.

[49] M. Frisch, G. Trucks, H. Schlegel, G. Scuseria, M. Robb, J. Cheeseman, J. Montgomery, T. Vreven, K. Kudin, J. Burant, J. Millam, S. Iyengar, J. Tomasi, V. Barone, B. Mennucci, M. Cossi, G. Scalmani, N. Rega, G. Petersson, H. Nakatsuji, M. Hada, M. Ehara, K. Toyota, R. Fukuda, J. Hasegawa, M. Ishida, T. Nakajima, Y. Honda, O. Kitao, H. Nakai, M. Klene, X. Li, J. Knox, H. Hratchian, J. Cross, V. Bakken, C. Adamo, J. Jaramillo, R. Gomperts, R. Stratmann, O. Yazyev, A. Austin, R. Cammi, C. Pomelli, J. Ochterski, P. Ayala, K. Morokuma, G. Voth, P. Salvador, J. Dannenberg, V. Zakrzewski, S. Dapprich, A. Daniels, M. Strain, O. Farkas, D. Malick, A. Rabuck, K. Raghavachari, J. Foresman, J. Ortiz, Q. Cui, A. Baboul, S. Clifford, J. Cioslowski, B. Stefanov, G. Liu, A. Liashenko, P. Piskorz, I. Komaromi, R. Martin, D. Fox, T. Keith, A. Laham, C. Peng, A. Nanayakkara, M. Challacombe, P. Gill, B. Johnson, W. Chen, M. Wong, C. Gonzalez, J. Pople, Gaussian 03, Revision C.02, (n.d.).

[50] D.A. Case, V. Babin, J. Berryman, R.M. Betz, Q. Cai, D.S. Cerutti, T.E. Cheatham III, T.A. Darden, R.E. Duke, H. Gohlke, A.W. Goetz, S. Gusarov, N. Homeyer, P. Janowski, J. Kaus, I. Kolossváry, A. Kovalenko, T.S. Lee, S. LeGrand, T. Luchko, R. Luo, B. Madej, K.M. Merz, F. Paesani, D.R. Roe, A. Roitberg, C. Sagui, R. Salomon-

Ferrer, G. Seabra, C.L. Simmerling, W. Smith, J. Swails, R.C. Walker, J. Wang, R.M. Wolf, X. Wu, P.A. Kollman, Amber 14, (2014). http://orbilu.uni.lu/handle/10993/16614 (accessed March 12, 2015).

[51] L. Zhang, J. Hermans, Hydrophilicity of cavities in proteins, Proteins Struct. Funct. Bioinforma. 24 (1996) 433–438. doi:10.1002/(SICI)1097-0134(199604)24:4<433::AID-PROT3>3.0.CO;2-F.

[52] T.H. Schmidt, C. Kandt, LAMBADA and InflateGRO2: Efficient Membrane Alignment and Insertion of Membrane Proteins for Molecular Dynamics Simulations, J. Chem. Inf. Model. 52 (2012) 2657–2669. doi:10.1021/ci3000453.

[53] W.L. Jorgensen, J. Chandrasekhar, J.D. Madura, R.W. Impey, M.L. Klein, Comparison of simple potential functions for simulating liquid water, J. Chem. Phys. 79 (1983) 926–935. doi:10.1063/1.445869.

[54] D. Bashford, K. Gerwert, Electrostatic calculations of the pKa values of ionizable groups in bacteriorhodopsin, J. Mol. Biol. 224 (1992) 473–486.

[55] A.M. Baptista, P.J. Martel, C.M. Soares, Simulation of electron-proton coupling with a Monte Carlo method: application to cytochrome c3 using continuum electrostatics, Biophys. J. 76 (1999) 2978–2998. doi:10.1016/S0006-3495(99)77452-7.

[56] H.J.C. Berendsen, D. van der Spoel, R. van Drunen, GROMACS: A message-passing parallel molecular dynamics implementation, Comput. Phys. Commun. 91 (1995) 43–56. doi:10.1016/0010-4655(95)00042-E.

[57] S. Pronk, S. Páll, R. Schulz, P. Larsson, P. Bjelkmar, R. Apostolov, M.R. Shirts, J.C. Smith, P.M. Kasson, D. van der Spoel, B. Hess, E. Lindahl, GROMACS 4.5: a high-throughput and highly parallel open source molecular simulation toolkit, Bioinforma. Oxf. Engl. 29 (2013) 845–854. doi:10.1093/bioinformatics/btt055.

[58] J.B. Klauda, R.M. Venable, J.A. Freites, J.W. O'Connor, D.J. Tobias, C. Mondragon-Ramirez, I. Vorobyov, A.D. MacKerell, R.W. Pastor, Update of the CHARMM All-Atom Additive Force Field for Lipids: Validation on Six Lipid Types, J. Phys. Chem. B. 114 (2010) 7830–7843. doi:10.1021/jp101759q.

[59] P. Bjelkmar, P. Larsson, M.A. Cuendet, B. Hess, E. Lindahl, Implementation of the CHARMM Force Field in GROMACS: Analysis of Protein Stability Effects from Correction Maps, Virtual Interaction Sites, and Water Models, J. Chem. Theory Comput. 6 (2010) 459–466. doi:10.1021/ct900549r.

[60] R.B. Best, X. Zhu, J. Shim, P.E.M. Lopes, J. Mittal, M. Feig, A.D. Mackerell, Optimization of the additive CHARMM all-atom protein force field targeting improved sampling of the backbone φ, ψ and side-chain χ(1) and χ(2) dihedral angles, J. Chem. Theory Comput. 8 (2012) 3257–3273. doi:10.1021/ct300400x.

[61] P.R. Magalhães, M. Machuqueiro, A.M. Baptista, Constant-pH Molecular Dynamics Study of Kyotorphin in an Explicit Bilayer, Biophys. J. 108 (2015) 2282–2290. doi:10.1016/j.bpj.2015.03.052.

[62] The PyMOL Molecular Graphics System, Version 1.7.4 Schrödinger, LLC., n.d.

[63] W. Humphrey, A. Dalke, K. Schulten, VMD: Visual molecular dynamics, J. Mol. Graph. 14 (1996) 33–38. doi:10.1016/0263-7855(96)00018-5.

[64] J.-F. Tomb, O. White, A.R. Kerlavage, R.A. Clayton, G.G. Sutton, R.D. Fleischmann, K.A. Ketchum, H.P. Klenk, S. Gill, B.A. Dougherty, K. Nelson, J. Quackenbush, L. Zhou, E.F. Kirkness, S. Peterson, B. Loftus, D. Richardson, R. Dodson, H.G. Khalak, A. Glodek, K. McKenney, L.M. Fitzegerald, N. Lee, M.D. Adams, E.K. Hickey, D.E. Berg, J.D. Gocayne, T.R. Utterback, J.D. Peterson, J.M. Kelley, M.D. Cotton, J.M. Weidman, C. Fujii, C. Bowman, L. Watthey, E. Wallin, W.S. Hayes, M. Borodovsky,

P.D. Karp, H.O. Smith, C.M. Fraser, J.C. Venter, The complete genome sequence of the gastric pathogen Helicobacter pylori, Nature. 388 (1997) 539–547. doi:10.1038/41483.

[65] R. Zufferey, E. Arslan, L. Thöny-Meyer, H. Hennecke, How replacements of the 12 conserved histidines of subunit I affect assembly, cofactor binding, and enzymatic activity of the Bradyrhizobium japonicum cbb3-type oxidase, J. Biol. Chem. 273 (1998) 6452–6459.

[66] J.-I. Oh, Effect of mutations of five conserved histidine residues in the catalytic subunit of the cbb3 cytochrome c oxidase on its function, J. Microbiol. Seoul Korea. 44 (2006) 284–292.

[67] L. Noodleman, W.-G. Han Du, J.A. Fee, A.W. Götz, R.C. Walker, Linking Chemical Electron–Proton Transfer to Proton Pumping in Cytochrome c Oxidase: Broken-Symmetry DFT Exploration of Intermediates along the Catalytic Reaction Pathway of the Iron–Copper Dinuclear Complex, Inorg. Chem. 53 (2014) 6458–6472. doi:10.1021/ic500363h.

[68] W.-G.H. Du, A.W. Götz, L. Yang, R.C. Walker, L. Noodleman, A broken-symmetry density functional study of structures, energies, and protonation states along the catalytic O–O bond cleavage pathway in ba3 cytochrome c oxidase from Thermus thermophilus, Phys. Chem. Chem. Phys. 18 (2016) 21162–21171. doi:10.1039/C6CP00349D.

**Highlights**

- Proton pathways in *cbb*3 (C-type) oxidase are explored by large-scale molecular dynamics simulations and continuum electrostatic calculations.
- The protonation state of H243 and conformational dynamics of Y223 and N289 control formation of protonic connections in the K*c*-channel.
- Proton uptake routes from the bulk to the entrance of the K*c*-channel involve E49P.
- A mechanism for proton pumping is proposed, with H337 as part of the proton-loading site.
- Three mutants - E49PA, T215A, and Y317F - are examined.